Transfer Between Invariant Manifolds: From Impulse Transfer to Low-Thrust Transfer

Maxime Chupin, Thomas Haberkorn, Emmanuel Trélat

From Impulse Transfer to Low-Thrust Transfer between Invariant Manifolds

Maxime Chupin*, Thomas Haberkorn†, Emmanuel Trélat‡

DOI:

In this work, a new method is developed to perform transfers that minimize fuel consumption between two invariant manifolds of periodic orbits in the Circular Restricted Three Body Problem. We start with an impulse transfer between two invariant manifolds to build an optimal control problem. This allows to choose an adequate fixed transfer time. Using the Pontryagin Maximum Principle, we formulate the resolution of the problem as that of finding the zero of a shooting function (indirect method). We develop an algorithm that couples different kinds of continuations (on cost, on final state, on thrust) to improve robustness and to initialize the solver. We illustrate the efficiency of the method with numerical examples. Finally, we study the influence of time transfer with a numerical study which, thanks to a continuation on this parameter, shows that when transfer duration goes to zero, the control converges to the impulse transfer that we started with. To the best of our knowledge, it is the first time that such a result is obtained.

I. Introduction

Since the late '70s, study of the Circular Restricted Three Body Problem (CRTBP) with the Libration Point Orbits has been of great interest. Indeed, several missions such as ISEE-3 (NASA) in 1978, SOHO (ESA-NASA) in 1996, GENESIS (NASA) in 2001, PLANK (ESA) in 2007 etc. have put this design knowledge into practice. A more profound understanding of the available mission options has also emerged due to the theoretical, analytical, and numerical advances in many aspects of libration point mission design.

There exists a huge number of references on the problem of determining low-cost trajectories by using the properties of the CRTBP and the properties of the equilibrium points called Lagrange or libration points (see [1] and references therein).

Concerning works that use the CRTBP model, we can notice that in the interesting works [2, 3], indirect method combined with continuation methods have been used to design missions from an Earth Geostationary Orbit to a Lunar Orbit. The minimum time problem is studied and solved, and continuations between energy minimization and fuel consumption minimization are performed.

Moreover, in [4], the developed methods involve the minimum-time problem, the minimum energy problem and the minimum fuel problem to reach a fixed point on a Halo orbit starting from a periodic orbit around Earth. Continuations on the thrust are used (indirect methods).

In [5, 6], the author recently developed an efficient method to compute an optimal low-thrust transfer trajectory in *finite* time without using invariant manifolds of the CRTBP. It is based on a three-step solution method using indirect methods and continuations methods and it gives good results.

In these last three contributions, manifolds are not used to help solving the formulated problem but invariant manifolds of the periodic orbits around libration points are a key concept to design interplanetary missions. For a complete point of view on the subject, we refer to [7–10].

These invariant manifolds are separatrices of the dynamics, and so, they can be interpreted as *gravitational currents* in the three body problem. In [11], and its extension in [12], the network of heteroclinic orbits is obtained. This gives us very interesting tools based on dynamical system methods to design free trajectories with prescribed itineraries.

For instance, the authors in [12–14] have developed very efficient methods to find "zero cost" trajectories between libration point orbits. They used dynamical system methods to construct heteroclinic orbits from invariant manifolds between Libration Point Orbits. These orbits have been used with impulse engines of spacecrafts to construct finite time transfers.

Following what was done for the patched conic approximation, we can connect (patch) restricted three body problems [15] and, thanks to invariant manifolds, it is possible to design a map of connections between various areas in the solar system. Indeed, intersections in the position variables between invariant manifolds can be computed and with an impulse, ΔV, it is possible to pass from one to another. This principle is the main tool to design the *Interplanetary Transport Network (ITN)* [16] which is a collection of gravitationally determined pathways through the Solar System that require very little energy for an object to follow.

However, the impulse needed to go from one invariant manifold to another cannot be achieved with a low-thrust engine. This is a question in its own, and the purpose of this work is to present a generic new method to address it.

Manifolds have been used in low-thrust mission in [17, 18]. The low-thrust propulsion is introduced by means of special attainable sets that are used in conjunction with invariant manifolds to define a first-guess solution. Then, they optimize their solution using an optimal control formalism. One can note that [19] is the first work that combines invariant manifolds and low-thrust in the Earth-Moon system.

In [19, 20], the authors develop direct optimization methods to address such issues. We refer the reader to the textbook [21] for direct methods in aerospace, and to [22] for a short description of the pros and cons of direct versus indirect approaches. In the present work, our objective is to develop an indirect (shooting) method combined with adequate continuations. Numerical homotopies are indeed a good way to overcome the main problem of the shooting method that is the difficulty to initialize it successfully (given that the domain of convergence of the underlying Newton method may be very small). In turn, we take advantage of the fastness and the good numerical accuracy of the shooting method, which is important in view of patching various three-body problems.

A lot of efforts have been done to design efficient methods to reach periodic orbits, Halo orbits, around equilibrium points in the three body problem. For example, in [23, 24], authors use indirect methods and direct multiple shooting methods to reach a manifold's insertion point that goes asymptotically a Halo orbit in the {Earth-Moon} system. Moreover, using transversality conditions, they optimize the insertion points on the manifold.

The outline for the article is as follows. In Sections II and III, we introduce the CRTBP and its properties such as LPOs and invariant manifolds. In Section IV, we recall the method to design trajectories with prescribed itineraries using invariant manifolds and impulse engines. In section V, we introduce the low-thrust model that does not allow for instantaneous changes in velocity. After that, we explain how we can use an impulse transfer to build an optimal control problem (Section VI). To do that we define both cost functions considered in this work (that we want to minimize): the L^1-norm of the control, which corresponds to the physical mass that we want to maximize but

*CEREMADE, Université Paris-Dauphine, PSL, chupin@ceremade.dauphine.fr

†MAPMO, Université d'Orléans, thomas.haberkorn@univ-orleans.fr

‡LJLL, Université Pierre et Marie Curie, emmanuel.trelat@upmc.fr

which is numerically difficult to optimize, and the L^2-norm of the control, which corresponds to the physical energy and is smoother. We introduce the continuation performed between these two related problems.

The last sections are about the numerical resolution of the previously formulated problems and the general method we developed. We use indirect methods based on the application of the Pontryagin Maximum Principle (PMP) [25–27], and because the main difficulty of these methods is to initialize them, we introduce other continuations for the final state and the thrust to improve robustness (Section VII). Note that the construction of the optimal control problem starting with the impulse transfer allows to choose an adequate fixed transfer time. The general algorithm is summarized in section VIII. In section IX, we present different numerical results for different CRTBP. We observe that the method is efficient and can be applied to various systems such as {Earth-Moon} or {Sun-Earth} systems.

In the method we present, one of the parameters that we fix is the transfer time. Of course, the larger the transfer time, the lower the cost (L^1-norm or L^2-norm). Moreover, it seems intuitive that the larger the time, the lower the maximum of the control norm during the transfer. A numerical study of the influence of this parameter is performed. Indeed, continuations on the *fixed* transfer time are computed from a (rather) large value to a near zero. It is shown that the control converges to the equivalent impulse transfer ΔV as the maximal thrust $T_{\max}$ goes to infinity. To the best of our knowledge, it is the first time that such a result is obtained.

For references on techniques used in our work such as continuation on cost, smoothing techniques and optimization techniques one can read [28–30] as well as [22] where the well-posedness of the continuations is proved.

Initialization of indirect methods with dynamical properties is a real challenge in order to improve the efficiency of indirect methods (see [22] and references therein). Indeed the main difficulties of such methods is to initialize the Newton-like algorithm, and the understanding of the dynamics can be very useful to construct an admissible trajectory for the initialization. Moreover, continuation methods as used in [31] or [32] are crucial to give robustness to these indirect methods.

The algorithm and the method we present in this work constitute a brick for designing interplanetary missions using invariant manifolds in order to take advantage of the Interplanetary Transport Network. A partial application of this algorithm is used in [33] to design a complete mission. This method could be a good first step to initialize missions patching three body problems with some uncontrolled parts (trajectories in invariant manifolds) and some controlled parts computed by this method to connect the invariant manifolds.

II. The Circular Restricted Three Body Problem

We use the paradigm of the Circular Restricted Three Body Problem. In this section we will follow the description by [1].

Let us consider a spacecraft in the field of attraction of Earth and Moon. We consider an inertial frame $\mathcal{I}$ in which the vector differential equation for the spacecraft's motion is written as:

$$m\frac{\mathrm{d}\underline{R}}{\mathrm{d}t} = -GM_1 m\frac{\underline{R}_{13}}{R_{13}^3} - GM_2 m\frac{\underline{R}_{23}}{R_{23}^3} \tag{1}$$

where M_1, M_2 and m are the masses respectively of Earth, Moon and the spacecraft, $\underline{R}$ is the spacecraft vector position, $\underline{R}_{13}$ is the vector Earth-spacecraft and $\underline{R}_{23}$ is the vector Moon-spacecraft. G is the gravitational constant. Let us describe the simplified general framework we will use.

Problem Description. To simplify the problem, and use a general framework, we consider the motion of the spacecraft P of negligible mass moving under the gravitational influence of the two masses M_1 and M_2, referred to as the primary masses, or simply the *primaries* (here Earth and Moon). We denote these primaries by P_1 and P_2. We assume that the primaries have circular orbits around their common center of mass. The particle P is free to move all around the primaries but cannot affect their motion.

The system is made adimensional by the following choice of units: the unit of mass is taken to be $M_1 + M_2$; the unit of length is chosen to be the constant distance between P_1 and P_2; the unit of time is chosen such that the orbital period of P_1 and P_2 about their center of mass is 2π. The universal constant of gravitation then becomes $G = 1$. The conversion from units of distance, velocity and time in the unprimed, normalized system to the primed, dimensionalized system is

$$\begin{array}{ll} \text{distance} & d' = l_* d, \\ \text{velocity} & s' = v_* s, \\ \text{time} & t' = \frac{t_*}{2\pi} t, \end{array} \tag{2}$$

where we denote by l_* the distance between P_1 and P_2, v_* the orbital velocity of P_1 and t_* the orbital period of P_1 and P_2.

We define the *mass parameter*

$$\mu = \frac{M_2}{M_1 + M_2}, \tag{3}$$

assuming that $M_1 > M_2$. We refer to [1] for the values of all the constants for various CRTBPs of the solar system.

Equations of Motion. If we write the equations in a rotating frame $\mathcal{R}$ in which the two primaries are fixed (the angular velocity is the angular velocity of their rotation around their center of mass, see [34]), we obtain that the coordinates of P_1 and P_2 are respectively

$$\xi_{P_1} = (-\mu, 0, 0, 0, 0, 0), \quad \xi_{P_2} = (1-\mu, 0, 0, 0, 0, 0).$$

Let us call $x_1^0 = -\mu$ and $x_2^0 = 1-\mu$, and by writing the state

$$\xi = (x, y, z, \dot{x}, \dot{y}, \dot{z})^T = (x_1, x_2, x_3, x_4, x_5, x_6)^T,$$

we obtain

$$\begin{cases} \dot{x_1} = x_4 \\ \dot{x_2} = x_5 \\ \dot{x_3} = x_6 \\ \dot{x_4} = x_1 + 2x_5 - (1-\mu)\dfrac{x_1 - x_1^0}{r_1^3} - \mu\dfrac{x_1 - x_2^0}{r_2^3} \\ \dot{x_5} = x_2 - 2x_4 - (1-\mu)\dfrac{x_2}{r_1^3} - \mu\dfrac{x_2}{r_2^3} \\ \dot{x_6} = -(1-\mu)\dfrac{x_3}{r_1^3} - \mu\dfrac{x_3}{r_2^3} \end{cases} \tag{4}$$

where

$$r_1 = \sqrt{\left(x_1 - x_1^0\right)^2 + x_2^2 + x_3^2} \quad \text{et} \quad r_2 = \sqrt{\left(x_1 - x_2^0\right)^2 + x_2^2 + x_3^2}$$

are respectively the distances between P and primaries P_1 and P_2.

We can define the potential

$$U(x_1, x_2, x_3) = -\frac{1}{2}\left(x_1^2 + x_2^2\right) - \frac{1-\mu}{r_1} - \frac{\mu}{r_2} - \frac{1}{2}\mu(1-\mu). \tag{5}$$

We denote by F_0 the vector field of the system and we define the energy of a state point as:

$$\mathcal{E}(\xi) = \frac{1}{2}(\dot{x}^2 + \dot{y}^2 + \dot{z}^2) + U(x, y, z). \tag{6}$$

III. Libration Point Orbits and Invariant Manifolds

In this Section, we recall some properties of the CRTBP. In particular, we introduce equilibrium points, Libration Points Orbits and invariant manifolds, for instance see [1, 33, 35–38].

A. Libration Point Orbits

The study of the CRTBP dynamical system shows that around the different equilibrium points of the vector field, there exists periodic orbits (and quasi-periodic orbits) called Libration Point Orbits. A lot of efforts has been dedicated for the theoritical and numerical study of such periodic orbits. We recall here some properties.

Equilibrium Points. The Lagrange points are the equilibrium points of the circular restricted three-body problem. Euler [39] and Lagrange [40] proved the existence of five equilibrium points: three collinear points on the axis joining the center of the two primaries, generally denoted by L_1, L_2 and L_3, and two equilateral points denoted by L_4 and L_5 (see figure 1).

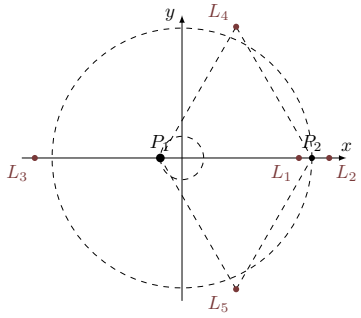

Figure 1: Lagrange points.

Computing equilateral points L_4 and L_5 is not complicated, but it is not possible to find exact solutions for collinear equilibria L_1, L_2 and L_3. A lot of efforts has been dedicated to find series expansion for these points. We used solutions from [41]. We recall that the collinear points are shown to be unstable (in every system), whereas L_4 and L_5 are proved to be stable under some conditions (see [42]).

Numerical computation. We use the method described in [33] to compute the libration point orbits around collinear Lagrange points. This method is based on a shooting method initialized with analytical approximations that can be found in [35–38].

In order to use these orbits to construct various missions, it is very useful to be able to compute the family of periodic orbits given by the well known Lyapunov-Poincaré theorem (see [42, 43]), providing us with different orbits that have different energies. To do that, we follow [33] and use a continuation method on the energy parameter.

We plot some examples of such periodic orbits in Figures 2 and 3.

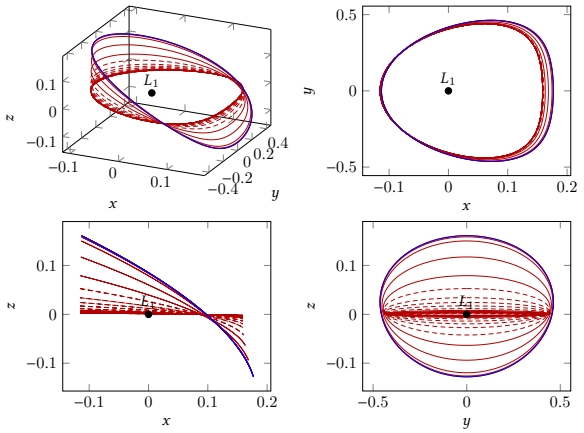

Figure 2: Family of Halo orbits in the {Sun-Earth} system in Richardson coordinates obtained by a Newton-like method and continuation on the energy. The first fixed excursion is $A_z = 240 \times 10^3$ km and the final energy is $-1.500\,42$ in normalized units (corresponding to a quasi-null z-excursion).

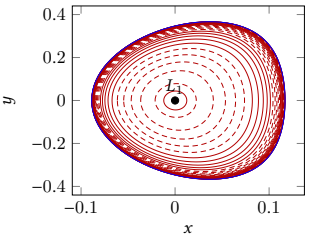

Figure 3: Family of planar Lyapunov orbits in the {Earth-Moon} system in Richardson coordinates obtained by a Newton-like method and continuation on the energy. The final energy is -1.6001 in normalized units.

B. Invariant Manifolds

All periodic orbits described in the previous section generate invariant manifolds, that is to say, the sets of phase points from which the trajectory converges to the periodic orbit, forward for the *stable* manifold and backward for the *unstable* manifold. These manifolds can be very useful to design interplanetary missions because as separatrices, they are some sort of gravitational currents. We refer to [1, chap. 4] for the proof of existence and a more detailed explanation of these manifolds and to [7–10]. For the sake of numerical reproducibility, we recall some well known properties.

Numerical Computation. Using the Poincaré map we can show that the eigenvectors corresponding to eigenvalues of the monodromy matrix are linear approximations of the invariant manifolds of the periodic orbit (see [1]).

The method to compute invariant manifolds is the following:

1. First, for ξ_0 a point on the periodic orbit, we compute the monodromy matrix and its eigenvectors. Let us denote by $Y^s(\xi_0)$ the normalized stable eigenvector and by $Y^u(\xi_0)$ the normalized unstable eigenvector.

2. Then, let
$$\begin{aligned} \xi^{s\pm}(\xi_0) &= \xi_0 \pm \alpha Y^s(\xi_0), \\ \xi^{u\pm}(\xi_0) &= \xi_0 \pm \alpha Y^u(\xi_0), \end{aligned} \tag{7}$$
be initial guesses for (respectively) the stable and unstable manifolds. The magnitude of α should be small enough to be within the validity of the linear estimate but not too small to keep a reasonable time of escape or convergence (for instance, see [44] for a discussion on the value of α).

3. Finally, we integrate numerically the unstable vector forward in time, using both α and $-\alpha$ to generate the two branches of the unstable manifold denoted by $W^{u\pm}(\xi_0)$. We do the same but backwards for the stable vector, and we get the two branches of stable manifold $W^{s\pm}(\xi_0)$.

In figure 4, we plot the four invariant manifolds for two Lyapunov orbits around L_1 and L_2 in the {Earth-Moon} system.

IV. Trajectories with Prescribed Itineraries

Invariant manifolds can be used to find trajectories with prescribed itineraries. To illustrate the method, we consider the planar motion of a spacecraft in the {Earth-Moon} system. We label the realm around Earth with $\mathcal{R}_E$, the realm around the Moon with $\mathcal{R}_M$ ant the exterior realm with $\mathcal{R}_X$ (see Figure 4). The different realms are defined with the Hill's region which a useful tool to design mission (see Hill's region in [1, 34]). Let us describe a method to find a trajectory with a prescribed itinerary.

Step 1. First, we choose an appropriate energy that allows for motion in the area that we want to reach. Assume that we want the particle to go between all three realms $\mathcal{R}_X$, $\mathcal{R}_M$ and $\mathcal{R}_E$, then we need to choose an energy greater than the one of the point L_2: for instance, $\mathcal{E} = -1.59$.

Step 2. We compute periodic orbits around the two equilibrium points L_1 and L_2 with energy $\mathcal{E}$. In Figure 4, we have computed two such Lyapunov orbits.

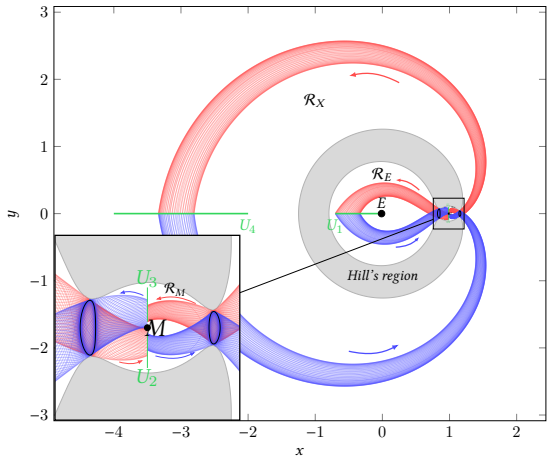

Figure 4: The eight invariant manifolds associated with the Lyapunov orbits of the points L_1 and L_2 in the {Earth-Moon} system, at a specific energy of $\mathcal{E} = -1.59$. The different Poincaré surfaces of section U_i are represented with the Hill's region.

Step 3. We define the four Poincaré surfaces of section (or Poincaré cuts) U_i, $i \in \{1, \dots, 4\}$. The surfaces are

$$\begin{aligned} U_1 &= \{(x, y, z);\ x < 0,\ y = 0\}, \\ U_2 &= \{(x, y, z);\ x = 1 - \mu,\ y < 0\}, \\ U_3 &= \{(x, y, z);\ x = 1 - \mu,\ y > 0\}, \\ U_4 &= \{(x, y, z);\ x < -1,\ y = 0\}. \end{aligned}$$

This way, the U_i are strategically placed (see [1]): if each U_i contains the (non empty) intersection between two of the invariant manifolds, then by computing it, we find a trajectory which connects different realms. This result is based on the fact that invariant manifolds are separatrices of the dynamics.

Step 4. We compute the invariant manifolds associated with the two periodic orbits as explained previously. We propagate them to the different Poincaré surfaces of section U_i, $i \in \{1, \dots, 4\}$ to obtain the intersection of each manifolds with the Poincaré cuts. Figure 4 presents the example of the {Earth-Moon} system. There are eight invariant manifolds, four for each of the two periodic orbits. Thanks to this method we are able, either to find a trajectory without any impulse respecting the prescribed itinerary, or, one with a finite number of impulses (for instance, when we can find an intersection in the positions of two invariant manifolds but with a velocity gap).

V. Modeling

A. Controlled Dynamics

We first describe the model for the evolution of our spacecraft in the CRTBP. In non normalized coordinates, the controlled dynamical system is

$$m(t)\frac{\mathrm{d}\underline{R}(t)}{\mathrm{d}t} = -GM_1 m(t)\frac{R_{13}(t)}{R_{13}^3(t)} - GM_2 m(t)\frac{R_{23}(t)}{R_{23}^3(t)} + T(t),$$

where T is the spacecraft driving force, and m is the time-dependent mass of the spacecraft. The equation of evolution of the mass is

$$\dot{m}(t) = -\beta \|T(t)\|,$$

where β is computed from two parameters I_{sp} and g_0: β is equal to $\frac{1}{I_{\mathrm{sp}} g_0}$ and its units is second per meter. We use the following values for these parameters

$$I_{\mathrm{sp}} = 2000\,\mathrm{s}, \quad \text{and} \quad g_0 = 9.81\,\mathrm{m/s^2}.$$

Moreover, the thrust is constrained as follows

$$\forall t, \|T(t)\| \leqslant T_{\max},$$

where $T_{\max} > 0$ is the maximal thrust that the engine can generate.

Using the normalization parameters, we denote by β_* the normalized counterpart of β and the coefficient $\frac{t_*^2}{4\pi^2 l_*} T_{\max}$ by ϵ. Furthermore, we write the thrust as $T(t) = \epsilon u(t)$ where for all t, $\|u(t)\| \leqslant 1$ in the normalized system. Hence, we get the dynamics:

$$\begin{cases} \dot{x}_1 = x_4 \\ \dot{x}_2 = x_5 \\ \dot{x}_3 = x_6 \\ \dot{x}_4 = x_1 + 2x_5 - (1-\mu)\dfrac{x_1 - x_1^0}{r_1^3} - \mu\dfrac{x_1 - x_2^0}{r_2^3} + \epsilon\dfrac{u_1}{m} \\ \dot{x}_5 = x_2 - 2x_4 - (1-\mu)\dfrac{x_2}{r_1^3} - \mu\dfrac{x_2}{r_2^3} + \epsilon\dfrac{u_2}{m} \\ \dot{x}_6 = -(1-\mu)\dfrac{x_3}{r_1^3} - \mu\dfrac{x_3}{r_2^3} + \epsilon\dfrac{u_3}{m} \\ \dot{m} = -\beta_* \epsilon \|u\| \end{cases}$$

In condensed form, we write the system as :

$$\begin{cases} \dot{x} = F_0(x) + \dfrac{\epsilon}{m}\displaystyle\sum_{i=1}^{3} u_i F_i(x), \\ \dot{m} = -\beta_* \epsilon \|u\|, \end{cases}$$

where F_0 is defined in (4) and

$$F_1(x) = \begin{pmatrix} 0 \\ 0 \\ 0 \\ 1 \\ 0 \\ 0 \end{pmatrix}, \quad F_2(x) = \begin{pmatrix} 0 \\ 0 \\ 0 \\ 0 \\ 1 \\ 0 \end{pmatrix}, \quad F_3(x) = \begin{pmatrix} 0 \\ 0 \\ 0 \\ 0 \\ 0 \\ 1 \end{pmatrix}.$$

Remark: This system belongs to a well known class of controlled systems: the affine control systems. F_0 is called a *drift vector field* while the F_i are called *control vector fields*. Let us note that for these systems, geometric control theory is helpful to establish controllability properties (see [45, 46]).

Controllability. In [2], it is proved that the CRTBP with a non evolving mass is controllable for a suitable subregion of the phase-space, denoted by X_μ^1, where the energy is greater than the energy of L_1:

Theorem 1 *For any $\mu \in (0, 1)$, for any positive ϵ, the circular restricted three-body problem with constant mass is controllable on X_μ^1.*

Thanks to [47, Prop. 2.2], one can extend this result to the system with an evolving mass.

VI. Construction of an Optimal Control Problem (OCP)

In the previous sections, we have recalled how a mission can be designed using *impulse* and *invariant manifolds* to save a lot of propellant. Invariant manifolds are separatrices of the dynamics and act as *gravitational currents*.

We introduced the model for the low-thrust engine spacecraft. Because of the low-thrust engine, the method presented in section IV for mission design cannot be applied. Indeed, to go from one invariant manifold to another, an instantaneous change of velocity is not possible anymore.

For this reason, we develop a method to connect two invariant manifolds using low-thrust. With this model, the natural context is optimal control theory. Indeed, because the control is permanent during the transfer time, one can write the minimization of the mass consumption in terms of an integral of the control norm.

First, let us introduce an optimal control problem to perform the transfer between two invariant manifolds.

A. From an Impulse Solution to an Optimal Control Problem

We start with an impulse transfer between two manifolds. We denote respectively by $\mathcal{M}_0$ and $\mathcal{M}_1$ the two invariant manifolds that we consider. The goal of this section is to find a trajectory performing the transfer between these two invariant manifolds.

Remark: The choice of the two invariant manifolds $\mathcal{M}_0$ and $\mathcal{M}_1$ depends on the complete mission that we want to design. Indeed, keep in mind that a transfer between two invariant manifolds can be viewed as the cornerstone of a complete mission design.

Of course, the two invariant manifolds should be chosen such that the transfer from one to another is useful. For example, they must be "oriented" in the same direction. Moreover, the two chosen invariant manifolds must be such that there exists a section where the distance in position and velocity is not too large.

These notions are not mathematically well defined here, but the key is the knowledge of the map of invariant manifolds.

B. The Impulse Transfer

We start with an impulse transfer between $\mathcal{M}_0$ and $\mathcal{M}_1$. We define a Poincaré surface of section denoted by U where there exists an intersection in position of the two invariant manifolds. Denote by $\xi_0^U = (\underline{x}_0^U, \underline{v}_0^U)$ and $\xi_1^U = (\underline{x}_1^U, \underline{v}_1^U)$ the two points in this surface of section where

$$\begin{aligned}\underline{x}_i^U &= (x_1^i, x_2^i, x_3^i) = (x_i, y_i, z_i), i \in \{0, 1\},\\ \underline{v}_i^U &= (x_4^i, x_5^i, x_6^i) = (\dot{x}_i, \dot{y}_i, \dot{z}_i), i \in \{0, 1\},\end{aligned}$$

and such that

$$\underline{x}_0^U = \underline{x}_1^U.$$

Denote by $\mathcal{A}_0$ (resp. $\mathcal{A}_1$) the orbit to which ξ_0^U (resp. ξ_1^U) belongs. Hence, to go from $\mathcal{A}_0$ belonging to $\mathcal{M}_0$ to $\mathcal{A}_1$ belonging to $\mathcal{M}_1$, we just have to perform the impulse

$$\Delta V = \underline{v}_1^U - \underline{v}_0^U.$$

Thanks to that, we are able to go from one orbit belonging to the first manifold to another belonging to the second manifold (see Figure 5).

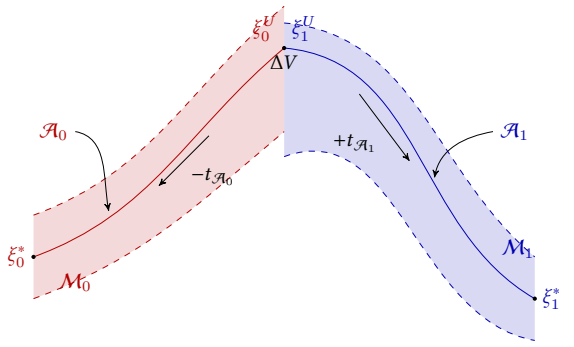

Figure 5: Drawing of the construction of the terminal points of the optimal control problem starting with an impulse transfer between invariant manifolds $\mathcal{M}_0$ and $\mathcal{M}_1$.

Intersection Problem. Different cases are in order:

1. If we consider *the planar case*, then there are four state variables ($\xi \in \mathbb{R}^4$) on the surface of section U, we look for an intersection in $\mathbb{R}^3$. Moreover, if both manifolds share the same energy, then a complete intersection in position and velocity is possible (not guaranteed). In that case, we do not need any control to perform the transfer. See the section on heteroclinic and homoclinic orbits in [1, 34].

2. If we consider *the planar case* but without the same energy, then it is possible to find a position intersection, but with a gap in velocity. Once again, the existence is only empirical.

3. If we consider *the spatial case*, then the state $\xi \in \mathbb{R}^6$ so on the surface of section U, we look for an intersection in $\mathbb{R}^5$. In that case, an intersection is difficult to find and, we actually give up searching for such a point. Instead, we restrict ourselves to finding an intersection in the position space. Note that the method we describe can be applied when there is no intersection (nor in position nor in velocity), but with a small

$$\Delta_\xi = (\Delta\underline{x}, \Delta V) = (\underline{x}_1^U - \underline{x}_0^U, \underline{v}_1^U - \underline{v}_0^U),$$

where $\underline{x} = (x_1, x_2, x_3) = (x, y, z)$ and $\underline{v} = (x_4, x_5, x_6) = (\dot{x}, \dot{y}, \dot{z})$ depending of the notation. For pedagogical reason, we consider the case where we only have a ΔV.

C. Optimal Control Problem

Thanks to the impulse transfer between the two invariant manifolds, we have two trajectories $\mathcal{A}_0 \in \mathcal{M}_0$ and $\mathcal{A}_1 \in \mathcal{M}_1$ and two points $\xi_0^U \in \mathcal{A}_0$ and $\xi_1^U \in \mathcal{A}_1$ such that

$$\xi_1^U - \xi_0^U = (0, \Delta V).$$

Perturbation Times. Starting with these two points $\xi_0^U \in \mathbb{R}^6$ and $\xi_1^U \in \mathbb{R}^6$, we choose two times $t_{\mathcal{A}_0}$ and $t_{\mathcal{A}_1}$ to respectively propagate backward the point ξ_0^U and forward the ξ_1^U. Mathematically, denoting by ϕ^{nat} the flow of the (uncontrolled) natural dynamics, we define two points in $\mathbb{R}^6$ by

$$\xi_0^* = \phi^{\text{nat}}(-t_{\mathcal{A}_0}, \xi_0^U), \quad \text{and} \quad \xi_1^* = \phi^{\text{nat}}(t_{\mathcal{A}_1}, \xi_1^U).$$

See Figure 5 for an illustration of this construction.

Optimal Control Problem Formulation. Let us define a new transfer time t_f such that

$$t_f = t_{\mathcal{A}_0} + t_{\mathcal{A}_1}.$$

We are now in a position to define the optimal control problem. We want to maximize the final mass (this in turn minimizes the amount of propellant burnt during the mission). Indeed, because the real cost for the launch of the spacecraft is to send it "away from Earth", *i.e.*, to send it to a first *parking orbit* around Earth (for example *a low Earth orbit* is the simplest and cheapest for spacecraft positioning), the lighter the spacecraft, the cheaper the launch.

The problem of the maximization of the final mass is equivalent to the minimization of the L^1-norm of the control u. Therefore the problem we want to solve is the following:

$$\mathcal{P}_{L^1} \begin{cases} C_{L^1}(u) = \displaystyle\int_0^{t_f} \|u\| \,\mathrm{d}t \to \min, \\ \dot{x} = F_0(x) + \dfrac{\epsilon}{m} \displaystyle\sum_{i=1}^{3} u_i F_i(x), \\ \dot{m} = -\beta_* \epsilon \|u\|, \\ \|u\| \leqslant 1, \\ x(0) = \xi_0^*, m(0) = m_0^*, \text{ and } x(t_f) = \xi_1^*. \end{cases} \tag{8}$$

Remark: Because we want to maximize the final mass, the transfer time must be fixed. Indeed, the larger the transfer time, the higher the final mass.

The choice of the transfer time is a difficult problem and thanks to the construction of the terminal points ξ_0^* and ξ_1^* (following the uncontrolled dynamics), we have fixed a transfer time which is adequate, in order to ensure that the problem that we address is indeed feasible.

D. Control Structure

1. *Minimization of the L^1-norm of the Control*

In this section, we apply the Pontryagin Maximum Principle (PMP) to the problem (8) to get the structure of the control (see [25–27]). We introduce the costate denoted by $(p^0, p, p_m) = (p^0, p_{\underline{x}}, p_{\underline{v}}, p_m)$ associated

with the state denoted by $(\xi, m) = (\underline{x}, \underline{v}, m)$. The Hamiltonian of the system is

$$\mathcal{H}(x, m, u, p^0, p, p_m) = (p^0 - \beta_* \epsilon p_m) \|u\| + H_0 + u_1 \frac{\epsilon}{m} H_1 + u_2 \frac{\epsilon}{m} H_2 + u_3 \frac{\epsilon}{m} H_3,$$

where $H_i = \langle p, F_i \rangle$ for $i \in \{0, \dots, 3\}$. The application of the PMP yields

$$\begin{aligned} \dot{x} &= \frac{\partial \mathcal{H}}{\partial p}(x, u, p), \\ \dot{p} &= -\frac{\partial \mathcal{H}}{\partial x}(x, u, p), \\ u(t) &= \arg\max_{\|v\| \leqslant 1} \mathcal{H}(x, m, v, p^0, p, p_m). \end{aligned}$$

In order to obtain the structure of the optimal control, we recall results from the contributions in [31, Prop. 2.3.] extended to the CRTBP in [3].

Thanks to these results, we are considering the normal case (see [48]), that is to say that $p^0 \neq 0$, so the costate (p^0, p) can be normalized with $p^0 = -1$.

We define $\varphi(p) = (H_1, H_2, H_3)$ and denoting by $\zeta = (x, m, p, p_m)$, let us introduce the *switching function*:

$$\psi(\zeta) = 1 - \beta_* \epsilon p_m - \frac{\epsilon}{m} \|\varphi(p)\|.$$

Then, the optimal control is:

- if $\|\varphi(p)\| \neq 0$, then

$$\begin{cases} u(\zeta) = 0 & \text{if } \psi(\zeta) < 0, \\ u(\zeta) = \alpha \frac{\varphi(p)}{\|\varphi(p)\|}, \ \alpha \in [0, 1] & \text{if } \psi(\zeta) = 0, \\ u(\zeta) = \frac{\varphi(p)}{\|\varphi(p)\|} & \text{otherwise,} \end{cases}$$

- if $\|\varphi(p)\| = 0$, then

$$\begin{cases} u(\zeta) = 0 & \text{if } \psi(\zeta) < 0, \\ u(\zeta) \in \mathbf{B}(0, 1) & \text{if } \psi(\zeta) = 0, \\ u(\zeta) \in \mathbf{S}(0, 1) & \text{otherwise,} \end{cases}$$

where $\mathbf{S}(a, b)$ is the $\mathbb{R}^3$-sphere centered in a with radius b, and $\mathbf{B}(a, b)$ is the $\mathbb{R}^3$ ball.

Remark: [Singular Arcs] Note that the case $\|\varphi(p)\| = 0$ can be a problem. However, one can prove that $\|\varphi(p)\|$ has a finite number of zeros along a solution and the assumption that it remains true on a neighborhood of the solution guarantees that the numerical evaluation of the control is not problematic as long as there are no singular arcs. Hence, we assume that *ψ has a finite number of zeros*.

This assumption can be checked *a posteriori*, once the numerical computation has been performed.

Shooting Function

We have established the structure of the control using the maximization condition of the PMP. Then, the resolution of the problem is equivalent to finding the root of a shooting function.

First, the free final mass transversality condition gives $p_m(t_f) = 0$. Because we consider fixed end points ξ_0^* and ξ_1^*, transversality conditions for the costate p associated to the state x do not give any information. The boundary value problem defined by the application of the PMP is reduced to find initial costate values $(p(0), p_m(0))$ such that the extremal solution $\zeta(\cdot) = (x(\cdot), m(\cdot), p(\cdot), p_m(\cdot))$ is well defined and reach the final state $x(t_f) = \xi_1^*$ starting at $(x(0), m(0)) = (\xi_0^*, m_0^*)$. Finally, the shooting function can be written as

$$\mathcal{S}_{L_1}(p(0), p_m(0)) = \begin{pmatrix} \phi^{\text{ext}}_{1,\dots,6}(\xi_0^*, m_0^*, p(0), p_m(0)) - \xi_1^* \\ \phi^{\text{ext}}_{14}(\xi_0^*, m_0^*, p(0), p_m(0)) \end{pmatrix} = \begin{pmatrix} 0 \\ 0 \end{pmatrix}$$

where ϕ^{ext} is the flow of the extremal dynamics given by the PMP.

To solve such a problem, we use a Newton-like method. For that kind of method, we need the shooting function to be differentiable. As noticed in [22, 28, 31], the shooting function remains differentiable in a neighborhood of an optimal trajectory under generic conditions (for instance, a neighborhood in which the same bang-bang structure is preserved).

With the assumption on singular arcs, the minimization of the L^1-norm of the control leads to a control called bang-bang*, indeed $\|u\|$ alternates between $\|u\| = 0$ and $\|u\| = 1$.*

Numerically, this problem is difficult to solve. Indeed, one has to know, a priori, the structure of the controlled solution, and the search for zeros of the shooting function is hard to initialize.

To overcome this difficulty, we use a continuation from a simpler problem: the L^2-norm of the control minimization.

2. *Minimization of the L^2-norm of the Control*

We consider the following problem

$$\mathcal{P}_{L^2} \begin{cases} C_{L^2}(u) = \displaystyle\int_0^{t_f} \|u\|^2 \, \mathrm{d}t \to \min, \\ \dot{x} = F_0(x) + \dfrac{\epsilon}{m} \displaystyle\sum_{i=1}^{3} u_i F_i(x), \\ \dot{m} = -\beta_* \epsilon \|u\|, \\ \|u\| \leqslant 1, \\ x(0) = \xi_0^*, m(0) = m_0^*, \text{ and } x(t_f) = \xi_1^*. \end{cases} \tag{9}$$

The problem is simpler because the optimal control is not *bang-bang* anymore (that will be clearer with the analysis of the structure of the optimal control) and we use it as the initial problem for a continuation to solve problem (8). Problem (9) has a cost defined by the L^2-norm of the control. This cost corresponds to the minimization of the energy.

For the sake of conciseness, we directly introduce the family of problems indexed by $\lambda \in [0, 1]$

$$\mathcal{P}_{C_\lambda} \begin{cases} C_\lambda(u) = \displaystyle\int_0^{t_f} \Big((1 - \lambda) \|u\|^2 + \lambda \|u\| \Big) \mathrm{d}t \to \min, \\ \dot{x} = F_0(x) + \dfrac{\epsilon}{m} \displaystyle\sum_{i=1}^{3} u_i F_i(x), \\ \dot{m} = -\beta_* \epsilon \|u\|, \\ \|u\| \leqslant 1, \\ x(0) = \xi_0^*, m(0) = m_0^*, \text{ and } x(t_f) = \xi_1^*. \end{cases} \tag{10}$$

Indeed, the analysis of the control structure is the same for problems (9) and (10) for $\lambda \in [0, 1[$. The Hamiltonians of these problems are

$$\mathcal{H}_\lambda(x, m, u, p^0, p, p_m) = (-\lambda - \beta_* \epsilon p_m) \|u\| - (1 - \lambda) \|u\|^2 + H_0 + u_1 \frac{\epsilon}{m} H_1 + u_2 \frac{\epsilon}{m} H_2 + u_3 \frac{\epsilon}{m} H_3. \tag{11}$$

We get the optimal control

- if $\|\varphi(p)\| \neq 0$, then

$$\begin{cases} u(\zeta) = 0 & \text{if } \psi_\lambda(\zeta) \leqslant 0, \\ u(\zeta) = \psi_\lambda(\zeta) \frac{\varphi(p)}{\|\varphi(p)\|} & \text{if } \psi_\lambda(\zeta) \in [0, 1], \\ u(\zeta) = \frac{\varphi(p)}{\|\varphi(p)\|} & \text{otherwise,} \end{cases} \tag{12}$$

- if $\|\varphi(p)\| = 0$, then

$$\begin{cases} u(\zeta) = 0 & \text{if } \psi_\lambda(\zeta) \leqslant 0, \\ u(\zeta) \in \mathbf{S}(0, \psi(\zeta)) & \text{if } \psi_\lambda(\zeta) \in [0, 1], \\ u(\zeta) \in \mathbf{S}(0, 1) & \text{otherwise,} \end{cases}$$

where $\mathbf{S}(a, b)$ is the $\mathbb{R}^3$-sphere centered in a with radius b.

The shooting function is exactly the same as before but the control is different, and so are the extremal dynamics. The result on the regularity of the shooting function still holds, because the shooting function for $\lambda < 1$ is more regular than the one for $\lambda = 1$ (the control is now continuous).

VII. Additional Continuations

We have now established the main results for the two problems that we want to solve: the L^1-norm minimization of the problem $(\mathcal{P}_{L^1})$, the L^2-norm minimization of the problem $(\mathcal{P}_{L^2})$ as well as all continuations between the two problems with the family of problems $(\mathcal{P}_{C_\lambda})$. This continuation is used in various references in different contexts such as two body problem (see [31]) and CRTBP (see [3]).

However, the transfer is still too difficult to initialize. Indeed, we still do not know how to initialize the simpler problem $\mathcal{P}_{L^2}$.

To achieve this, we combine several continuations that are of different kinds: one on the final state, another one on the maximal value of the thrust, and another one on the cost functional. The overall method is a good way for automatically initializing the solving. The order in which the continuations are performed is important (some paths do not work). The structure of the algorithm is represented in Figure 7.

We introduce in this section the two additional continuations we use in the complete algorithm.

A. Final State Continuation

Let us start with the first continuation in our multistep method. We consider the problem described in Section A, that is to say, with the L^2-norm of the control as the cost function $(\mathcal{P}_{L^2})$.

Instead of the final state ξ_1^*, we consider the point ξ_1^{nat} defined by

$$\xi_1^{\text{nat}} = \phi^{\text{nat}}(t_f, \xi_0^*).$$

In simple words, we have just propagated the initial point by following the natural dynamics during the transfer time. See Figure 6 for an illustration. It is obvious then that we know how to solve the optimal control problem $(\mathcal{P}_{L^2})$ with $\xi_1^* = \xi_1^{\text{nat}}$.

Indeed, a *constant null control*, with a null costate, constitutes the optimal extremal solution which follows the natural dynamics.

We can then construct a continuation of problems to solve $\mathcal{P}_{L^2}$. We define the following family of problems depending continuously on the parameter $\lambda \in [0, 1]$ (see Figure 6 for an illustration)

$$\mathcal{P}_{\text{FS}}^\lambda \begin{cases} C_{L^2}(u) = \displaystyle\int_0^{t_f} \|u\|^2 \,\mathrm{d}t \to \min, \\ \dot{x} = F_0(x) + \dfrac{\epsilon}{m} \displaystyle\sum_{i=1}^{3} u_i F_i(x), \\ \dot{m} = -\beta_* \epsilon \|u\|, \\ \|u\| \leqslant 1, \\ x(0) = \xi_0^*, m(0) = m_0^*, \text{ and } x(t_f) = (1-\lambda)\xi_1^{\text{nat}} + \lambda \xi_1^*. \end{cases}$$

This problem is associated to the corresponding shooting function

$$\mathcal{S}_{\text{FS}}^\lambda(p(0), p_m(0)) = \begin{pmatrix} \phi^{\text{ext}}_{1,\dots,6}(\xi_0^*, m_0^*, p(0), p_m(0)) - \xi_1^\lambda \\ \phi^{\text{ext}}_{14}(\xi_0^*, m_0^*, p(0), p_m(0)) \end{pmatrix} = \begin{pmatrix} 0 \\ 0 \end{pmatrix},$$

where

$$\xi_1^\lambda = (1-\lambda)\xi_1^{\text{nat}} + \lambda \xi_1^*.$$

B. Thrust Continuation

The low level of the thrust is also an issue. Indeed, the lower the magnitude of the maximal thrust, the smaller the attainable set, and so the more difficult the problem is to initialize. To overcome this difficulty, we use another continuation, but this time, on the maximal thrust.

Let ϵ_{obj} be the maximal thrust corresponding to the real engine that we want to use for the transfer. We also consider a greater thrust ϵ_{init}. For instance, consider the example of ϵ_{obj} corresponding to 0.3 N and ϵ_{init} corresponding to 60 N. We denote by

$$\epsilon_\lambda = (1-\lambda)\epsilon_{\text{init}} + \lambda \epsilon_{\text{obj}},$$

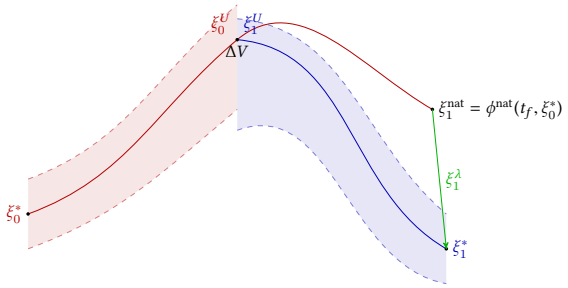

Figure 6: Illustration of the continuation on the final state. ξ_1^{nat} is the propagation of the initial point ξ_0^* during the transfer time t_f. Step by step, we reach the final point $\xi_1^\lambda = (1-\lambda)\xi_1^{\text{nat}} + \lambda\xi_1^*$, with λ going from 0 to 1.

the intermediary thrust that allows us to define the following family of problems for all $\lambda \in [0, 1]$.

$$\mathcal{P}_{\text{thrust}}^\lambda \begin{cases} C_{L^2}(u) = \displaystyle\int_0^{t_f} \|u\|^2 \,\mathrm{d}t \to \min, \\ \dot{x} = F_0(x) + \dfrac{\epsilon_\lambda}{m} \displaystyle\sum_{i=1}^{3} u_i F_i(x), \\ \dot{m} = -\beta_* \epsilon_\lambda \|u\|, \\ \|u\| \leqslant 1, \\ x(0) = \xi_0^*, m(0) = m_0^*, \text{ and } x(t_f) = \xi_1^*. \end{cases}$$

VIII. Description of the Algorithm: From Impulse Transfer to Low-Thrust Transfer

We designed an algorithm (implemented in C++) to solve the problem of performing the transfer between two *natural* trajectories of two invariant manifolds (but not only). In this section, we briefly describe the algorithm.

A. Principle

The main idea is described by the following items and summarized in Figure 7.

- We start with the two points denoted by ξ_0^U and ξ_1^U in Section A and Figure 5. These points are chosen in such a way that they minimize the distance between the two intersections between invariant manifolds and the Poincaré cut we chose.
- We give two times of propagation $t_{\mathcal{A}_0}$ and $t_{\mathcal{A}_1}$ to build the end-points of the transfer and an additional parameter $\alpha_T \in]0, 1]$. This parameter allows to start the resolution with two points denoted by $\xi_0^{\alpha_T}$ and $\xi_1^{\alpha_T}$ and defined as

  $$\xi_0^{\alpha_T} = \phi(-\alpha_T t_{\mathcal{A}_0}, \xi_0^U), \quad \text{and} \quad \xi_1^{\alpha_T} = \phi(\alpha_T t_{\mathcal{A}_1}, \xi_1^U).$$

  The two times of propagation $t_{\mathcal{A}_0}$ and $t_{\mathcal{A}_1}$ define a total *fixed* transfer time for the problem: $t_f = t_{\mathcal{A}_0} + t_{\mathcal{A}_1}$.

  These two points are closer than the two end-points defined as

  $$\xi_0^* = \phi(-t_{\mathcal{A}_0}, \xi_0^U), \quad \text{and} \quad \xi_1^* = \phi(t_{\mathcal{A}_1}, \xi_1^U)$$

  We then reach the two objective states ξ_0^* and ξ_1^* by continuation on the initial and final state as described in Section A.[a]
- A (boolean) parameter is given to activate the continuation between the minimization of the L^2-norm of the control and the minimization of the L^1-norm. If it is active, then, to overcome some numerical difficulties, we add another parameter, to indicate the position of this continuation in the algorithm (see Figure 7).

[a] The continuation on the initial state can easily be derived from the explanation of the final state continuation.

- If we give two different maximal thrusts, the algorithm performs a continuation on the thrust as explained in Section B.

- Checking the L^i-norm of the control ($i \in \{1, 2\}$) during the thrust continuation, we can verify if the border of the accessible set is reached (or at least get an indication of whether this is the case). If so, then we allow for an increase in the transfer time by another continuation on this parameter.

Of course, we allow for the initialization of a non zero costate to help convergence of the first step of the algorithm.

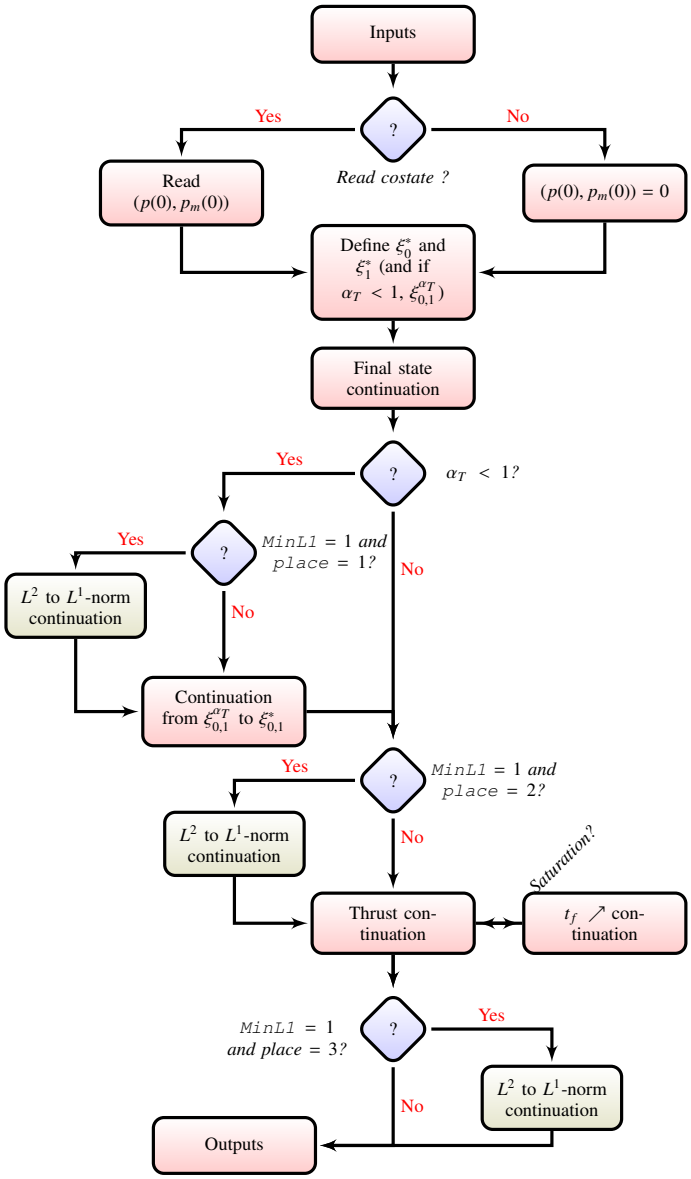

Figure 7: Description of the algorithm to solve the transfer between invariant manifolds with low thrust.

1. *Numerical Codes*

Although there exists excellent software to perform continuations for optimal control problem such as the well-known Hompack90 [49] or Hampath [32], because of the structure of the algorithm we developed, we chose to write our own code.

We implemented our code in C++, with interfaces to some very efficient FORTRAN codes. We used:

- the DOP853 explicit step-varying Runge-Kutta method developed by [50]. To verify our implementation of the method we developed, we added another integrator, `ode.f`, by Shampine and Gordon, which can be found on the `netlib.org` website.

- For the Newton-like method, we used the well known FORTRAN code: the MINPACK subroutine HYBRD by Burton S. Garbow, Kenneth E. Hillstrom, Jorge J. More. One can find a F90 version `hbrd.f`, by A. Miller. These two versions are implementations of Powell's Hybrid algorithm used to solve systems of nonlinear equations.

Note that we have not used automatic differentiation for the computation of the costate dynamics and for the variational equation associated to the Hamiltonian flow. We could have used, for instance, the very efficient software TAPENADE [51]. Because the costate dynamics are quite simple, and thanks to the efficiency of the implementation of Powell's Hybrid algorithm (which does not require the jacobian), we did not need to use this tool.

IX. Numerical Results

In this section, we apply the method that we developed to real transfers between invariant manifolds.

A. Transfer between Invariant Manifolds: {Earth-Moon} System, Halo Orbits

Let us consider once again the {Earth-Moon} system, and two Halo orbits around L_1 and L_2 with different energies. In table 1, we give the initial conditions and the periods for the two considered Halo orbits. These two Halo orbits have been computed with the same z-excursion of 16×10^3 km. We refer to [1] for the values of all the constants for various CRTBPs of the solar system.

	x	y	z
Halo L_1	8.23362033247E-01	0.0E+00	4.16230924917E-05
Halo L_2	1.12040065667E+00	0.0E+00	4.16230924917E-05
	$\dot{x}$	$\dot{y}$	$\dot{z}$
Halo L_1	0.0E+00	1.26343508887E-01	0.0E+00
Halo L_2	0.0E+00	1.76071039637E-01	0.0E+00
	Period		
Halo L_1	2.74294400617E+00		
Halo L_2	3.41558381117E+00		

Table 1: Initial conditions and periods for the two Halo orbits around L_1 and L_2 used to perform the transfer between their invariant manifolds. Values are expressed in the normalized system of units of the {Earth-Moon} system.

We follow the method that was previously described:

1. We compute the manifolds from the two periodic orbits around L_1 and L_2. Here, we consider Halo orbits (which are diffeomorphic to a circle). See Figure 2 for a plot of such an orbit.

2. We compute the intersections with the Poincaré cut U_2. See Figure 8. We plot the different projections onto the (y, z)-plane (recall that x is set to $1 - \mu$ on U_2), the $(y, \dot{y})$-plane and the $(z, \dot{z})$-plane.

3. We find the two points ξ_0^U and ξ_1^U that minimize $\Delta\xi = \left\|\xi_0^U - \xi_1^U\right\|$. Note that we obtain not only a $\Delta V = \Delta \underline{v}$ but also a $\Delta \underline{x}$. Indeed, we observe in Figure 8 that there is no intersection in the projections onto the $(y, \dot{y})$-plane.

4. We choose two times, previously denoted by $t_{\mathcal{A}_0}$ and $t_{\mathcal{A}_1}$. Here, we choose 0.5 for both times, expressed in the normalized system of units. This corresponds to a total travel time of 4.34 days. Thanks to this choice, the two end-points can be built. We denote them by ξ_0^* and ξ_1^*. The two natural trajectories are plotted in Figure 9.

The final state continuation ($\mathcal{P}_{\text{FS}}^{\lambda}$) is straightforward as long as the maximal thrust is large enough. In Figure 10a, we plot the norm of the control during each step of the final state continuation, and we note that

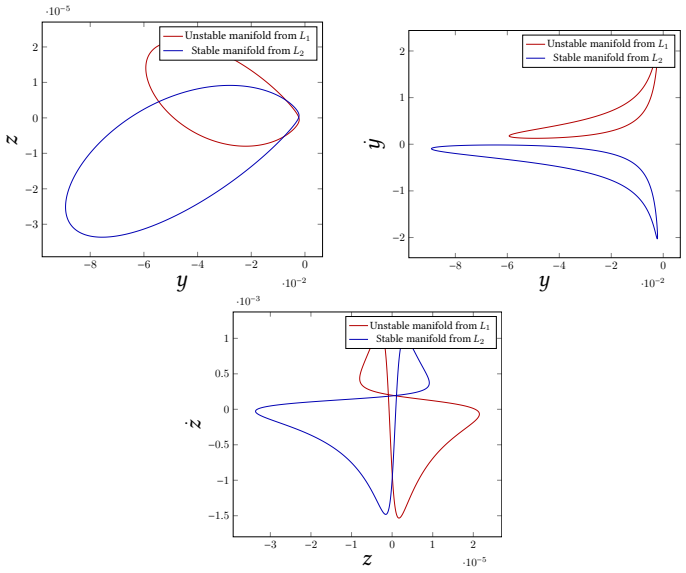

Figure 8: {Earth-Moon} system: Different projections of the intersection with the Poincaré cut U_2 for the invariant manifolds associated with the two Halo orbits around L_1 and L_2. Note that there is no intersection between the two manifolds, and this is obvious with the $(y, \dot{y})$-plane projection.

even though the final control is smaller than 0.55 N, it reaches nearly 3 N during the continuation.

We compute the transfer starting with a maximal thrust of 60 N to reach 0.45 N by the continuation ($\mathcal{P}^{\lambda}_{\text{thrust}}$). See Figure 10b for the plot of the evolution of the control norm with respect to time during the continuation. We observe that the control is saturated only along the last step of the continuation. Indeed, for a maximal thrust greater than 0.55 N, the control is not saturated, and so, the continuation on the maximal thrust does not change the optimal control, until reaching the critical value. One can think that it is useless to start this continuation with the value of 60 N, but, for instance, if we start with a value of 1 N, the final state continuation fails. Even though the control is not saturated, a large starting value provides us with a suitable attainable set, and allows the final state continuation to converge. This way the continuation on the thrust is very fast, and smooth.

The continuation on the cost ($\mathcal{P}_{C_\lambda}$) between the L^2-norm and the L^1-norm is then performed and succeeds easily. The different steps in the continuation for the norm of the control are plotted in Figure 10c.

The final trajectories are plotted in Figure 9. The trajectories for both the L^1-minimization and the L^2-minimization are very close to each other and differences cannot be seen on the plot. Obviously, the longer we have to perform the transfer (that is to say the choice of $t_{\mathcal{A}_0}$ and $t_{\mathcal{A}_1}$), the smaller both the L^1-cost and L^2-cost are.

Because we are using exclusively indirect methods, the computation of the transfer, including all steps and continuations, only takes 13.18 s on a standard desktop computer. Each of the three continuations is very efficient, and they converge in, respectively, 19, 20 and 22 iterations. We used an initial mass of 1500 kg for the spacecraft, and the final mass is 1492.885 68 kg for the minimization of the L^1-norm of the control.

Remark: This transfer method can be used to design a complete mission initialized with several controlled and uncontrolled parts, the uncontrolled ones being trajectories belonging to invariant manifolds.

This is the idea of this work: we want to use, as explained in the introduction, the invariant manifolds in the Interplanetary Transport Network [16], connected by small optimal transfers between invariant manifolds, to initialize the complete mission. The final mission will consist of several uncontrolled parts (following the invariant manifolds) and controlled parts (the connection between manifolds computed with our algorithm).

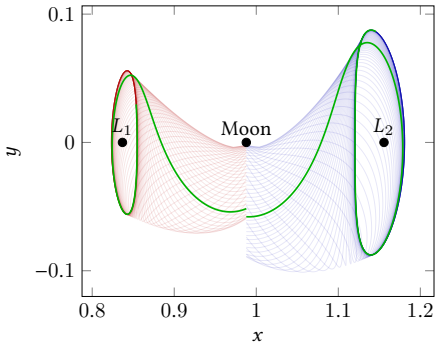

(a) Intersection of the two invariant manifolds, and the two trajectories that correspond to ξ_0^U and ξ_1^U that minimize the distance between the two sections.

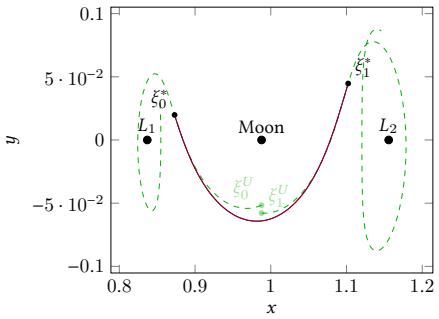

(b) Optimal solutions for the transfer between the two invariant manifolds. The solutions for the minimization of the L^2-norm of the control and the solution for the L^1-norm overlap because of the tiny difference between them.

Figure 9: {Earth-Moon} system: Construction and solving of the transfer problem between the two invariant manifolds of two Halo orbits around L_1 and L_2.

B. Transfer between Invariant Manifolds: {Sun-Earth} System, Halo Orbits

This time we consider the {Sun-Earth} system, and two Halo orbits around L_1 and L_2 with different energies, respectively $\mathcal{E}_{L_1} = -1.500444$ and $\mathcal{E}_{L_2} = -1.500443$. In table 2, we give the initial conditions and the periods for the two considered Halo orbits. Once again, we refer to [1] for the values of all the constants for various CRTBPs of the solar system.

	x	y	z
Halo L_1	9.88877586385E-01	0.0E+00	4.01075229212E-06
Halo L_2	1.00838140029E+00	0.0E+00	1.61657961732E-05
	$\dot{x}$	$\dot{y}$	$\dot{z}$
Halo L_1	0.0E+00	8.79724315850E-03	0.0E+00
Halo L_2	0.0E+00	9.75059689672E-03	0.0E+00
	Period		
Halo L_1	3.06024482087E+00		
Halo L_2	3.10252118223039E+00		

Table 2: Initial conditions and periods for the two Halo orbits around L_1 and L_2 used to perform the transfer between their manifolds. Values are expressed in the normalized system of unit of the {Sun-Earth} system.

Once again, we follow exactly the same method, and perform the computation as easily as in the previous case. We plot the different projections of the intersection with the Poincaré cut U_2 in Figure 11.

As previously, we compute the two terminal points ξ_0^U and ξ_1^U that minimize the distance between the two invariant manifolds and we choose the normalized time of propagation (backward and forward) to build the end-points of the transfer ξ_0^* and ξ_1^*. See Figure 12 for the plot of the manifolds and the two *natural* trajectories (*i.e.* without control).

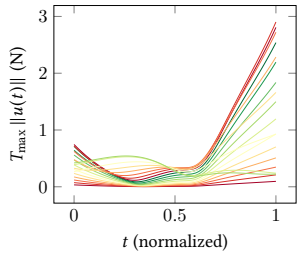

(a) Norm of the control in Newton during the final state continuation. (19 iterations)

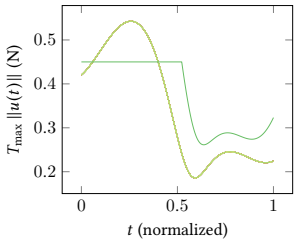

(b) Norm of the control in Newton during the thrust continuation. Before reaching a maximal thrust below 0.55 N nothing changes. The last step of the continuation saturates the control. (20 iterations)

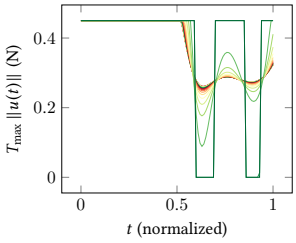

(c) Norm of the control in Newton during the continuation from the L^2-norm of the control to the L^1-norm. We finally get a bang-bang control. (22 iterations)

Figure 10: Different continuations during the resolution of the transfer between invariant manifolds in the {Earth-Moon} system.

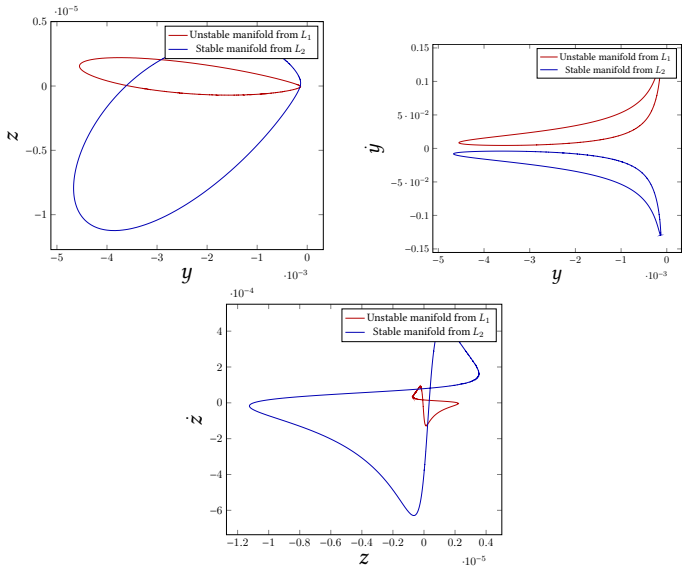

Figure 11: {Sun-Earth} system: Different projections of the intersection with the Poincaré cut U_2 for the invariant manifolds associated with the two Halo orbits around L_1 and L_2. Note that there is no intersection between the two manifolds, this is obvious on the $(y, \dot{y})$-plane projection.

Here, we have chosen $t_{\mathcal{A}_0} = t_{\mathcal{A}_1} = 0.5$. This corresponds to approximately 58 days in total. We choose a starting thrust of 60 N to reach a targeted thrust of 0.3 N.

The final state continuation is smooth and fast thanks to the rather large initial maximal thrust (see Figure 13a). Then, the thrust continuation is easier than for the {Earth-Moon} system, indeed, here we never reach the maximal thrust, and so, this continuation does not change the control at all (see Figure 13b).

The continuation between the L^2-minimization and the L^1-minimization is straightforward. Note that we obtain a different structure for the bang-bang control, and here, we do not start this continuation with a saturated control.

Finally, we obtain an optimal trajectory. As before, the initial mass is 1500 kg, and the final mass is 1490.1144 kg. The computational time on a standard desktop computer is 21.86 s for the entire computation of the transfer (from initial states computation to the last continuation on the cost). The final optimal trajectory is plotted in Figure 12 and the different controls for the different continuations are plotted in Figure 13.

C. Study of the Transfer Time Parameter

We have seen that one of the parameters we fix is the transfer time. Of course, the larger the transfer time, the lower the cost (L^1-norm or L^2-norm). Moreover, it seems intuitive that the larger the time, the lower the maximum of the control norm during the transfer. We perform a numerical study of the influence of this parameter for the two transfers previously introduced: the transfer between invariant manifolds from Halo orbits in the {Sun-Earth} and {Earth-Moon} systems.

We vary the time parameter to test in different cases the efficiency of our algorithm. We consider the states ξ_0^U and ξ_1^U defined for the two transfer problems as the two states minimizing the distance in position and velocity (see Section A). We then choose a sequence $\left(t_f^i\right)_{i\in\{1,\dots,N\}}$ discretizing interval $[0.001, 2.914]$ and we execute the algorithm for each t_f^i. Using the notation defined in the previous section, we choose for all $i \in \{1, \dots, N\}$,

$$t^i_{\mathcal{M}_0} = t^i_{\mathcal{M}_0} = \frac{t_f^i}{2}.$$

The method is efficient and succeeds for almost every t_f^i. We plot in Figure 14 three sets of tests for the {Sun-Earth} system and in Figure 15 for the {Earth-Moon} system. First, we plot the control for small times, when the norm of the control is high and looks like an impulse ΔV. The second set is a control for longer times (similar to the control obtained in the previous section). We observe that when we increase the transfer time, the method fails for a certain time interval. For the {Earth-Moon} system, the interval is

$$I_{EM} = [1.724, 2.224]$$

and for the {Sun-Earth} system the interval is

$$I_{SE} = [2.126, 2.526].$$

Note that these two intervals are discrete approximations. If we pass this interval, then the method succeeds again but it gives a different structure of the control and we observe that the optimal trajectories obtained have one revolution around the second primary (respectively Earth and Moon). There is a bifurcation in the structure of the optimal trajectory with respect to the time parameter. We plot the different trajectories for the two systems in 16a and 16b.

The time parameter is crucial. We have to pick it very carefully to obtain the desired result. Note that, whereas there is an interval in which our method fails, it succeeds for a very large range and so, it is not difficult to pick a suitable time using the method described in section VIII.

Finally, because one can expect that when the transfer time goes to zero ($t_f \to 0$), the control converge to the equivalent ΔV corresponding to an impulse transfer, in Figure 17, we plotted the sequence η_i defined by

$$\eta_i = \left\| \int_0^{t_f^i} \epsilon_* \frac{\|u(t)\|}{m(t)} \mathrm{d}t - \Delta V \right\|,$$

where ΔV is defined by

$$\Delta V = \left\| \underline{v}_0^U - \underline{v}_1^U \right\|,$$

with $\xi_0^U = (\underline{x}_0^U, \underline{v}_0^U)$ and $\xi_1^U = (\underline{x}_1^U, \underline{v}_1^U)$

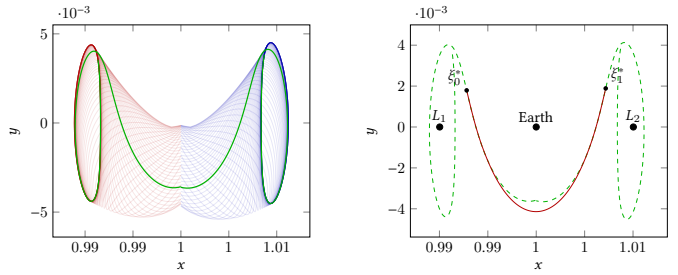

(a) Intersection of the two invariant manifolds, and the two trajectories that correspond to the two computed points ξ_0^U and ξ_1^U that minimize the distance between the two sections.

(b) Optimal solutions for the transfer between the two invariant manifolds. The solutions for the minimization of the L^2-norm of the control and the solution for the L^1-norm overlap because of the tiny difference between them.

Figure 12: {Sun-Earth} system: Construction and solution of the transfer problem between the two invariant manifolds of two Halo orbits around L_1 and L_2.

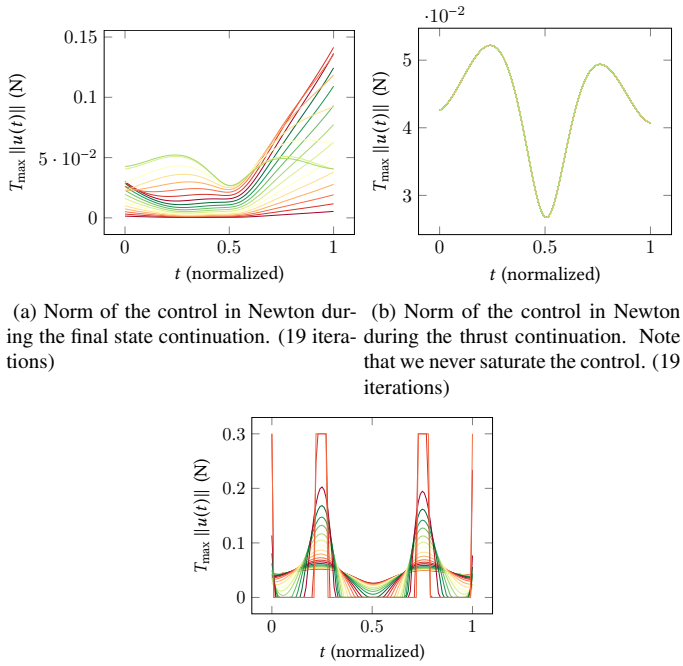

(a) Norm of the control in Newton during the final state continuation. (19 iterations)

(b) Norm of the control in Newton during the thrust continuation. Note that we never saturate the control. (19 iterations)

(c) Norm of the control in Newton during the continuation from the L^2-norm of the control to the L^1-norm. We eventually get a bang-bang control. (25 iterations)

Figure 13: Different continuations during the resolution of the transfer between invariant manifolds in the {Sun-Earth} system.

We observe that in both considered examples, the control converges to the ΔV when the transfer time decreases. Note that, because there is also a $\Delta \underline{x}$ for the {Earth-Moon} example, we can expect that the convergence may not be to ΔV exactly. However, the main gap concerns the velocity, hence, in both case the Figure 17 shows that when t_f goes to 0, then $\eta_i \to 0$. This is coherent with the construction of the problem recalling that we have designed an optimal control problem starting with an impulse transfer between the two invariant manifolds.

Conclusion

To conclude, we have designed a general algorithm (and a software written in C++) that performs the transfer between two invariant manifolds. This relies on a few parameters that we have to choose. Of course, because we minimize the norm of the control (L^2 or L^1), we have to fix the transfer time. This is a crucial parameter. The study of the influence of this parameter should be done more precisely. Indeed, we know that the longer the transfer time is, the smaller the cost is, but the drawback is that when we choose too long a transfer time, the first final state continuation can fail. We have seen that there exist some values of time for which our method fails but these times are sort of transition times between two structures of the trajectory with or without a revolution around the second primary. Outside these time interval, the method is robust and succeeds for a large range of transfer times. Moreover, we observe that when the transfer time goes to 0, it seems that the control converges to the impulse control as expected. To the best of our knowledge, it is the first time that such a result is obtained. Finally, on our two experiments, we observe that the behavior with respect to the time parameter is independent of the CRTBP we consider.

We think that this algorithm and this method constitute a brick for designing interplanetary missions using invariant manifolds, and more precisely the Interplanetary Transport Network. A partial application of this algorithm is used in [33] for a complete mission. We think that it could be a good first step to initialize missions patching three body problems with some uncontrolled parts (trajectories in invariant manifolds) and some controlled parts computed by this method to connect the invariant manifolds.

References

[1] Koon, W. S., Lo, M. W., Marsden, J. E., and Ross, J. E., *Dynamical Systems, the Three-Body Problem, And Space Mission Design*, Springer-Verlag New York Inc, 2006.

[2] Caillau, J.-B. and Daoud, B., "Minimum Time Control of the Restricted Three-Body Problem," *SIAM Journal on Control and Optimization*, Vol. 50, No. 6, 2012, pp. 3178–3202.

[3] Caillau, J.-B., Daoud, B., and Gergaud, J., "Minimum fuel control of the planar circular restricted three-body problem," *Celestial Mech. Dynam. Astronom.*, Vol. 114, No. 1-2, 2012, pp. 137–150.

[4] Zhang, C., Topputo, F., Bernelli-Zazzera, F., and Zhao, Y.-S., "Low-Thrust Minimum-Fuel Optimization in the Circular Restricted Three-Body Problem," *Journal of Guidance, Control, and Dynamics*, Vol. 38, No. 8, 2015, pp. 1501–1510, doi: 10.2514/1.G001080.

[5] Epenoy, R., "Optimal long-duration low-thrust transfers between libration point orbits," *IAC-2012*, 2012.

[6] Epenoy, R., *Recent Advances in Celestial and Space Mechanics*, chap. Low-Thrust Transfers Between Libration Point Orbits Without Explicit Use of Manifolds, Springer International Publishing, Cham, 2016, pp. 143–178.

[7] Gómez, G., Llibre, J., Martí nez, R., and Simó, C., *Dynamics and mission design near libration points. Vol. I*, Vol. 2 of *World Scientific Monograph Series in Mathematics*, World Scientific Publishing Co., Inc., River Edge, NJ, 2001, Fundamentals: the case of collinear libration points, With a foreword by Walter Flury.

[8] Gómez, G., Simó, C., Llibre, J., and Martí nez, R., *Dynamics and mission design near libration points. Vol. II*, Vol. 3 of *World Scientific Monograph Series in Mathematics*, World Scientific Publishing Co., Inc., River Edge, NJ, 2001, Fundamentals: the case of triangular libration points.

[9] Gómez, G., Simó, C., Llibre, J., and Martí nez, R., *Dynamics and mission design near libration points. Vol. II*, Vol. 3 of *World Scientific Monograph Series in Mathematics*, World Scientific Publishing Co., Inc., River Edge, NJ, 2001, Fundamentals: the case of triangular libration points.

[10] Gómez, G., Jorba, A., Simó, C., and Masdemont, J., *Dynamics and mission design near libration points. Vol. IV*, Vol. 5 of *World Scientific Monograph Series in Mathematics*, World Scientific Publishing Co., Inc., River Edge, NJ, 2001, Advanced methods for triangular points.

[11] Conley, C. C., "Low Energy Transit Orbits in the Restricted Three-Body Problems," *SIAM Journal on Applied Mathematics*, Vol. 16, No. 4, 1968, pp. 732–746.

[12] Koon, W. S., Lo, M. W., Marsden, J. E., and Ross, S. D., "Heteroclinic connections between periodic orbits and resonance transitions in celestial mechanics," *Chaos: An Interdisciplinary Journal of Nonlinear Science*, Vol. 10, No. 2, 2000, pp. 427–469.

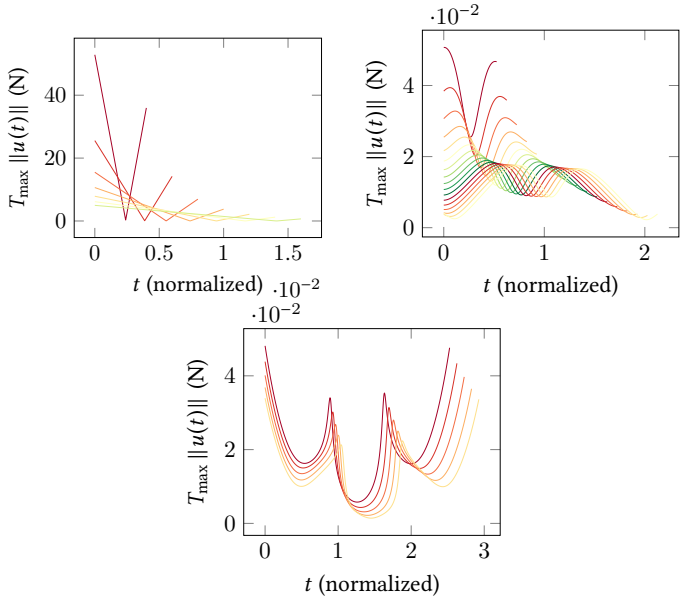

Figure 14: Controls for different transfer times for the transfer between invariant manifolds from Halo orbits in the {Sun-Earth} system. Left: Small times, similar to ΔV. Center: Longer times. Right: After the interval I_{SE}, where the algorithm fails, we get a different structure for the control corresponding to a trajectory with a revolution.

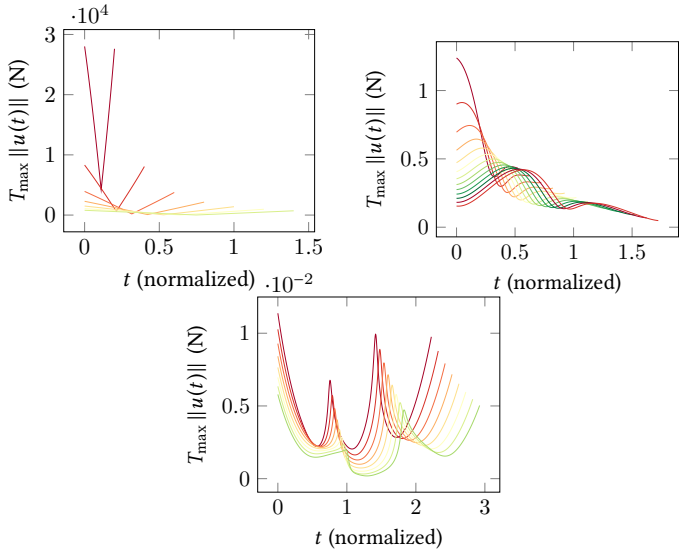

Figure 15: Controls for different transfer time for the transfer between invariant manifolds from Halo orbits in the {Earth-Moon} system. Left: small times, similar to ΔV. Center: Longer times. Right: After the interval I_{SE}, where the algorithm fails, we get a different structure for the control corresponding to a trajectory with a revolution.

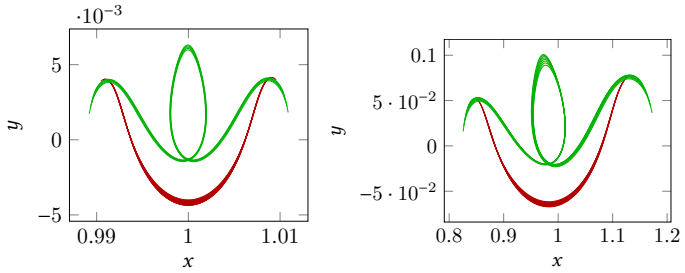

(a) For the {Sun-Earth} system. (b) For the {Earth-Moon} system.

Figure 16: Different optimal trajectories for the two considered systems. We observe a bifurcation when the time increases, after respectively I_{SE} and I_{EM}, the trajectories perform a revolution around the second primary.

[13] Gomez, G. and Masdemont, J., "Some Zero Cost Transfers between Libration Point Orbits," *POINT ORBITS, AAS PAPER 00-177, AAS/AIAA ASTRODYNAMICS SPECIALIST CONFERENCE*, 2000.

[14] Zazzera, F. B., Topputo, F., and Massari, M., "Assessment of mission design including utilisation of libration points and weak stability boundaries," Tech. Rep. 03-4103b, European Space Agency, the Advanced Concepts Team, 2004, Available on line at www.esa.int/act.

[15] Belbruno, E. A. and Miller, J. K., "Sun-perturbed Earth-to-moon transfers with ballistic capture," *Journal of Guidance Control Dynamics*, Vol. 16, Aug. 1993, pp. 770–775.

[16] Ross, S. D., "The interplanetary transport network," *American Scientist*, Vol. 94, No. 3, 2006, pp. 230–237.

[17] Mingotti, G., Topputo, F., and Bernelli-Zazzera, F., "Low-energy, low-thrust transfers to the Moon," *Celestial Mechanics and Dynamical Astronomy*, Vol. 105, No. 1-3, 2009, pp. 61–74.

[18] Mingotti, G., Topputo, F., and Bernelli-Zazzera, F., "Optimal Low-Thrust Invariant Manifold Trajectories via Attainable Sets," *Journal of guidance, control, and dynamics*, Vol. 34, 2011, pp. 1644–1655.

[19] Mingotti, G., Topputo, F., and Bernelli-Zazzera, F., "Combined Optimal Low-Thrust and Stable-Manifold Trajectories to the Earth-Moon Halo Orbits," *AIP Conference Proceedings*, Vol. 886, No. 1, 2007, pp. 100–112.

[20] Martin, C. and Conway, B. A., "Optimal Low-Thrust Trajectories Using Stable Manifolds," *Spacecraft Trajectory Optimization*, edited by B. A. Conway, Cambridge University Press, 2010, p. 238–262, Cambridge Books Online.

[21] Betts, J. T., *Practical Methods for Optimal Control Using Nonlinear Programming*, SIAM, 2001.

[22] Trélat, E., "Optimal control and applications to aerospace: some results and challenges," *J. Optim. Theory Appl.*, Vol. 154, No. 3, 2012, pp. 713–758.

[23] Senent, J., Ocampo, C., and Capella, A., "Low-Thrust Variable-Specific-Impulse Transfers and Guidance to Unstable Periodic Orbits," *Journal of Guidance, Control, and Dynamics*, Vol. 28, No. 2, 2005, pp. 280–290, doi: 10.2514/1.6398.

[24] Ozimek, M. T. and Howell, K. C., "Low-Thrust Transfers in the Earth-Moon System, Including Applications to Libration Point Orbits," *Journal of Guidance, Control, and Dynamics*, Vol. 33, No. 2, 2010, pp. 533–549, doi: 10.2514/1.43179.

[25] Pontryagin, L., Boltianski, V., Gamkrélidzé, R., and Michtchenko, E., *Théorie mathématique des processus optimaux*, 1974.

[26] Lee, E. B. and Markus, L., *Foundations of optimal control theory*, Robert E. Krieger Publishing Co., Inc., Melbourne, FL, 2nd ed., 1986.

[27] Trélat, E., *Contrôle optimal*, Mathématiques Concrètes. [Concrete Mathematics], Vuibert, Paris, 2005, Théorie & applications. [Theory and applications].

[28] Haberkorn, T., *Transfert orbital a poussee faible avec minimisation de la consommation: resolution par homotopie differentielle*, Thèse de doctorat, Institut National Polytechnique de Toulouse, Toulouse, France, octobre 2004.

[29] Jiang, F., Baoyin, H., and Li, J., "Practical Techniques for Low-Thrust Trajectory Optimization with Homotopic Approach," *Journal of Guidance, Control, and Dynamics*, Vol. 35, No. 1, 2012, pp. 245–258, doi: 10.2514/1.52476.

[30] Bertrand, R. and Epenoy, R., "New smoothing techniques for solving bang–bang optimal control problems—numerical results and statistical interpretation," *Optimal Control Applications and Methods*, Vol. 23, No. 4, 2002, pp. 171–197.

[31] Gergaud, J. and Haberkorn, T., "Homotopy Method for minimum consumption orbit transfer problem," *ESAIM : Control, Optimisation and Calculus of Variations*, Vol. 12, No. 2, avril 2006, pp. 294–310.

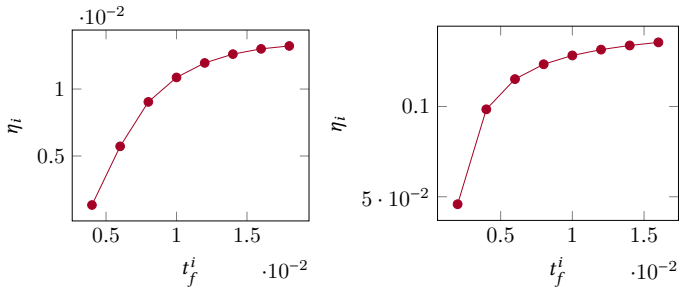

(a) For the {Sun-Earth} system. (b) For the {Earth-Moon} system.

Figure 17: Evolution of the sequence $(\eta_i)_{i\in I}$. In both cases, we observe that the cost converges to the impulse when the transfer time goes to zero.

[32] Cots, O., Caillau, J.-B., and Gergaud, J., "Differential pathfollowing for regular optimal control problems," *Optim. Methods Software*, Vol. 27, No. 2, 2012, pp. 177–196.

[33] Chupin, M., Haberkorn, T., and Trélat, E., "Low-Thrust Lyapunov to Lyapunov and Halo to Halo Missions with L^2-Minimization," *ESAIM: Mathematical Modelling and Numerical Analysis*, June 2016, accepted.

[34] Chupin, M., *Interplanetary transfers with low consumption using the properties of the restricted three body problem*, Theses, Université Pierre et Marie Curie - Paris VI, Oct. 2016, tel-01389197.

[35] Richardson, D. L., "Analytic Construction of periodic orbits about the collinear points," Vol. 22, No. 3, oct 1980.

[36] Archambeau, G., Augros, P., and Trélat, E., "Eight-shaped Lissajous orbits in the Earth-Moon system," *Mathematics in Action*, Vol. 4, No. 1, 2011, pp. 1–23.

[37] Jorba, À. and Masdemont, J., "Dynamics in the center manifold of the collinear points of the Restricted Three Body Problem," 1997.

[38] Farquhar, R. W. and Kamel, A. A., "Quasi-periodic orbits about the translunar libration point," *Celestial mechanics*, Vol. 7, No. 4, 1973, pp. 458–473.

[39] Euler, L., "De motu rectilineo trium corpörum se mutuo attrahentium," Vol. Oeuvres, Seria Secunda tome XXv Commentationes Astronomicae, 1767, pp. 144–151.

[40] Lagrange, J.-L., "Essai sur le problème des trois corps," Vol. Oeuvres de Lagrange 6, Gauthier-Villars, 1772, pp. 272–282.

[41] Szebehely, V. G., *Theory of Orbits - The Restricted Problem of Three Bodies*, Academic Press, 1967.

[42] Meyer, K., Hall, G., and Offin, D., *Introduction to Hamiltonian Dynamical Systems and the N-Body Problem*, Applied Mathematical Sciences, Springer New York, 2010.

[43] Bonnard, B., Faubourg, L., and Trélat, E., *Mécanique céleste et contrôle des véhicules spatiaux*, Vol. 51 of *Mathématiques & Applications (Berlin) [Mathematics & Applications]*, Springer-Verlag, Berlin, 2006.

[44] Gómez, G., Masdemont, J., Simó, C., and Jorba, A., "Study Refinement of Semi-analytical Halo Orbit Theory: Executive Summary," *ESOC Contract No.: 8625/89/D/MD (SC)*, 1991.

[45] Jurdjevic, V., *Geometric Control Theory*, Cambridge Studies in Advanced Mathematics, Cambridge University Press, 1997.

[46] Bonnard, B., Caillau, J.-B., and Trélat, E., "Geometric optimal control of elliptic Keplerian orbits," *Discrete Contin. Dyn. Syst. Ser. B*, Vol. 5, No. 4, 2005, pp. 929–956.

[47] Caillau, J.-B. and Noailles, J., "Coplanar control of a satellite around the Earth," *ESAIM Control Optim. Calc. Var.*, Vol. 6, 2001, pp. 239–258.

[48] Bonnard, B. and Chyba, M., *Singular Trajectories and Their Role in Control Theory*, Mathématiques et Applications, Springer, 2003.

[49] Watson, L., *HOMPACK90: FORTRAN 90 Codes for Globally Convergent Homotopy Algorithms*, Department of Computer Science, Virginia Polytechnic Institute and State University, 1996.

[50] Hairer, E., Nørsett, S., and Wanner, G., *Solving Ordinary Differential Equations I: Nonstiff Problems*, Springer Series in Computational Mathematics, Springer Berlin Heidelberg, 2008.

[51] Hascoët, L. and Pascual, V., "The Tapenade Automatic Differentiation tool: Principles, Model, and Specification," *ACM Transactions On Mathematical Software*, Vol. 39, No. 3, 2013.